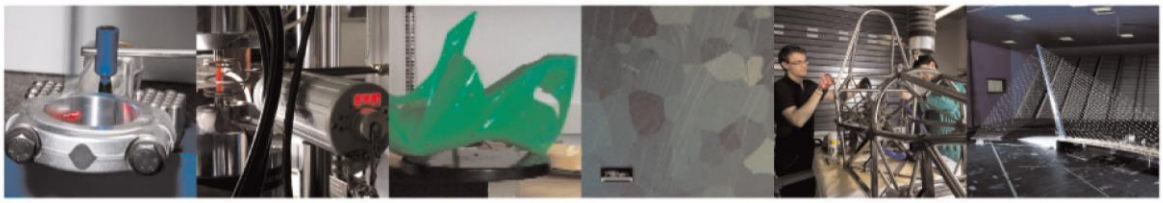

Sub-micrometric surface texturing of AZ31 Mg-alloy through two-beam direct laser interference patterning with a ns-pulsed green fiber laser

Furlan, Valentina; Biondi, Marco; Demir, Ali Gökhan; Pariani, Giorgio; Previtali, Barbara; Bianco, Andrea

This is a post-peer-review, pre-copyedit version of an article published in APPLIED SURFACE SCIENCE. The final authenticated version is available online at:
http://dx.doi.org/10.1016/j.apsusc.2017.06.138

DIPARTIMENTO DI MECCANICA ■ POLITECNICO DI MILANO
via G. La Masa, 1 ■ 20156 Milano ■ EMAIL (PEC): pecmecc@cert.polimi.it
http://www.mecc.polimi.it
Rev. 0

Sub-micrometric surface texturing of AZ31 Mg-alloy through Two-beam Direct Laser Interference Patterning with a ns-pulsed green fiber laser

Valentina Furlan[1*], valentina.furlan@polimi.it
Marco Biondi[1], marco.biondi@mail.polimi.it
Ali Gökhan Demir[1], aligokhan.demir@polimi.it
Giorgio Pariani[2], giorgio.pariani@brera.inaf.it
Barbara Previtali[1], barbara.previtali@polimi.it
Andrea Bianco[2], andrea.bianco@brera.inaf.it

[1] Department of Mechanical Engineering, Politecnico di Milano, Via La Masa 1, 20156 Milan, Italy
[2] INAF – Osservatorio astronomico di Brera, Via E. Bianchi 46, 23807 Merate, Lecco, Italy
*Corresponding author

Sub-micrometric surface texturing of AZ31 Mg-alloy through Two-beam Direct Laser Interference Patterning with a ns-pulsed green fiber laser

Valentina Furlan[1*], valentina.furlan@polimi.it

Marco Biondi[1], marco.biondi@mail.polimi.it

Ali Gökhan Demir[1], aligokhan.demir@polimi.it

Giorgio Pariani[2], giorgio.pariani@brera.inaf.it

Barbara Previtali[1], barbara.previtali@polimi.it

Andrea Bianco[2], andrea.bianco@brera.inaf.it

[1]Department of Mechanical Engineering, Politecnico di Milano, Via La Masa 1, 20156 Milan, Italy

[2]INAF – Osservatorio astronomico di Brera, Via E. Bianchi, 46, 23807 Merate, LC, Italy

*Corresponding author

Abstract

Two-beam direct laser interference patterning (DLIP) is the method that employs two beams and provides control over the pattern geometry by regulating the angle between the beams and the wavelength of the beam. Despite the simplistic optical arrangement required for the method, the feasibility of sub-micrometric patterning of a surface depends on the correct manipulation of the process parameters, especially in the case of metallic materials. Magnesium alloys from this point of view exhibit further difficulty in processability due to low melting point and high reactivity. With biocompatibility and biodegradability features, Mg-alloy implants can further advantage of surface structuring for tailoring the biological behaviour.

In this work, a two-beam DLIP setup has been developed employing an industrial grade nanosecond-pulsed fiber laser emitting at 532 nm. The high repetition rate and ramped pulse profile provided by the laser were exploited for a more flexible control over the energy content deposited over the heat-sensitive Mg-alloy. The paper describes the strategies developed for controlling ramped laser emission at 20 kHz repetition rates. The process feasibility window was assessed within a large range of parameters. Within the feasibility window, a complete experimental plan was applied to investigate the effect of main laser process parameters on the pattern dimensions. Periodic surface structures with good definition down to 580 nm ± 20 nm spacing were successfully produced.

Keywords: Surface sub-micrometric patterning; laser surface texturing; biodegradable implant; magnesium alloy; green laser

1 Introduction

Hierarchically patterned surfaces are capable of providing multiple functionalities exploitable in different fields, such as optical systems, biomedical, microelectronics or in automotive ones [1],[2]. Several techniques for the fabrication of periodic micro and nano structures have been developed like optical lithography [3], electron-beam [4], microcontact printing [5] and replica moulding [6]. These methods reach high pattern resolution, but they normally require multiple steps in order to produce the final microstructure. As a consequence, artefacts such as loss of information or pattern distortion may arise.

On the other hand, the use of laser source to produce surface structures and patterns has been widely studied. Different laser methods were proposed in order to obtain sub-micrometric and nano-manufacturing, which can involve addition or subtraction of materials [7],[8],[9]. Laser synthesis of nano-materials like nanoparticles, nanotubes and nanowires were studied. In laser synthesis methods, a laser beam is focused inside a controlled environment on a material substrate. Material ablation leads to micro- and nano- particle generation [9]. These approaches cannot be easily manipulated to be used as surface modification techniques. Two-photon polymerisation (TPP) is a more common example of processing technology used for sub-micron to micrometric structures. TTP can be realized using a pulsed laser source to achieve high fluence and ultra short pulse duration [9]. A focused beam is used in order to guarantee the solidification of liquid polymer layer. The process enables intrinsic capability to obtain structured surfaces on the realized component due to its high resolution. However, it still remains as a costly and slow option. Another method, which involves the use of laser to obtain a surface modification from micrometric up to nanometric scale is the laser interference lithography (LIL). LIL is realized by interference of coherent beams whose intensity distribution is recorded by a photosensitive layer and it is later transferred by thermal and chemical processes to the substrate [1],[9]. LIL can be realized with short and ultrashort pulsed laser source. A comparison between fs and ns system with LIL method showed that higher feature resolution was possible with fs lasers, but larger textured areas were achieved with ns pulsed lasers due to the higher coherence length [10]. However, despite LIL applicability on large-area production, it requires multiple steps in order to produce the final structures and the process is slow and time consuming.

Considering the limitations of described methods, the attention is focused on methods which involve the use of laser in direct laser writing (DLW), which is easily adaptable to an industrial environment due to its simplicity. Direct Laser Writing (DLW) involves the use of a pulsed laser beam for ablating the material surface in order to generate the desired periodic patterns, such as lines, micro-holes and defined dimples [1],[7]. However, in DLW, the size of the features is commonly limited by the dimension of the diffraction limited focused beam, which remains in micrometric region. Sub-micrometric laser induced periodic surface structures (LIPSS) can be obtained indirectly by employing DLW with ps and fs laser sources[2],[8]. Employing this method, ripples, bumps and conical structures were obtained on different materials. Their dimension can range between a few nanometres to micrometric scale, depending on materials and laser parameters. On the other hand, despite a defined directionality, dimension and geometry of LIPSS are not easily controllable since their formation relies mainly on the used laser parameters [2],[8]-[12]. In order to overcome dimensional limits of DLW approach, a recent advancement in the field of micro and sub-micrometric surface texturing using a laser source involves Direct Laser Interference Patterning

(DLIP) technique. DLIP is achieved through the superimposition of two or more coherent and polarized laser beams, commonly generated by the same laser source, which redistribute the laser beam profile with a periodic interference structure. The difference in the intensity of regions under constructive and destructive interference results in a preferential removal of the material through ablation and vaporization when high power pulsed laser sources are exploited. Periodical patterns types (e.g. lines, dots, columnar or hexagonal structures) are directly related to number of interfering beams [1],[13]. The period of the periodic structures is controlled by the relative angle between the interference beams and by the laser wavelength. For two laser beams interference, the period of fringes (Λ [nm]) is computed as follow [1]:

$$\Lambda = \frac{\lambda}{2\sin(\frac{\theta}{2})} \quad \text{Eq. 1}$$

where λ [nm] is the laser wavelength and θ [°] is the angle between the interfering beams. DLIP is a single step process, since no development of a photo-resist and/or an etching are required, with the consequent advantage in terms of production time. Several works were dedicated to develop DLIP with different pulsed laser sources applied to different materials, due to its advantages [14]-[16]. Nanosecond pulsed lasers are the most employed in DLIP technique, generally with a selection or a control by a shutter element of a single pulse passage. Solid-state laser sources were commonly used, coupled to wavelength harmonic generator. A large number of papers dealt with DLIP applied to polymeric materials [17]- [20]. Nevertheless, metallic materials were also investigated focusing on melting and re-solidification phenomena [16],[21],[22].

Several works focused on the applications of surfaces structured by DLIP. DLIP was investigated in tribology to improve the performance of lubricating films [13],[23], in organic solar cells applications to change optical concentration [20], in optoelectronics devices to improve transmittance performance and thermo- electrical behaviour [24],[25],[26]. Furthermore, an increased interest in use of laser texturing techniques for biomedical applications was recently observed. Indeed, several works showed how the realization of an interference pattern onto polymeric materials promote the cells adhesion and proliferation or avoid the bacteria adhesion [27]-[30]. On the other hand, the use of DLIP on metallic materials for biomedical applications has received a lot less attention from the research communities. Linear periodic structures have been generated with DLIP on titanium implants in order to improve biological performance of dental implants [31], but there is a lack in the treatment of biodegradable metals. As a matter of fact, surface engineering and texturing of biodegradable metals has received much less attention in general compared to their permanent counterparts. The more common direct laser writing approach has been widely applied in the past on more conventional metals for permanent implants in order to control their biomedical performance [32]. Biodegradable alloys possess different limitations in laser processing, which require further attention.

Mg alloys constitute the most widely studied group of biodegradable metals. A main drawback of Mg alloys is related to the high degradation rate. Laser surface treatments were investigated in order to control corrosion rate, by grain refinement and material microstructure modification [33],[34]. Control over the surface wettability of Mg alloys can be advantageous for corrosion protection, for protective coating application and also for controlling the biological interaction between the implant and the tissue [35],[36]. On the other hand, DLIP can constitute an alternative option for achieving sub-micrometric and periodic surface structures on Mg alloys in a deterministic way. Such structures can be beneficial for manipulating the cell-surface interactions at the implantation stage. Cell

attachment and proliferation can be controlled by the aid of these structures especially in stent applications.
In this work, an industrial nanosecond fiber laser source with a ramp profile emission is used for fabricating micrometric and sub-micrometric structures by two-beam interference patterning on AZ31 magnesium alloy. In particular the paper tackles two important points for the processing of the biodegradable Mg alloy. The first one is related to the low melting point and high reactivity of the material, which lowers the processability by pulsed lasers and lowers the process precision. The second aspect is connected to the use of an industrial laser source, which is characterized by a pulse train emission profile. The inability in single pulse selection constitutes a further complexity. DLIP process as well as pattern quality were investigated as a function of different trains of pulses. Results showed that micrometric to sub-micrometric periodic surface structures could be obtained with high feature definition once the stable processing strategies were developed.

2 Modelling

2.1 Beam intensity distribution in two-beam interference

In two-beam interference, the intensity distribution of the electric field can be expressed as [37]:

$$I = I_1 + I_2 + 2\sqrt{I_1 \cdot I_2}\cos(\varphi) \quad \text{Eq. 2}$$

where I_1 and I_2 are respectively the intensities of first and second beams, φ is the phase difference between two beams. Considering a balance of the intensities, namely $I_1 = I_2$, the expression is simplified as follow:

$$I = 2 \cdot I_1[\,1 + \cos(\varphi)] \quad \text{Eq. 3}$$

when $\cos(\varphi) = 1$, in the condition of two beams perfect beams constructive interference, $I = 4I_1$. In this work, $I_1 = I_2 = I_0/2$, where I_0 is laser beam intensity before its splitting, obtaining $I = 2I_0$.

2.2 Laser ablation with interfering beams and multiple pulses

DLIP process consists in laser ablation with a shaped beam intensity profile. In order to investigate the trend of the fluence, both laser light features and the interaction with the material should be considered. It is possible determine the peak fluence of a Gaussian beam as follow:

$$F = \frac{2E_p}{\pi w_0^2} \quad \text{Eq. 4}$$

where E_p is the peak energy and w_0 is the beam waist radius at focal position which contains 86% of laser energy [UNI EN ISO 11146]. Starting from Eq.4, it is possible determine the formulation of the average fluence (F_m) in a pulse train for a generic beam size (w_s) positioned at Δz, as:

$$F_m(N) = \frac{2E_m(N)}{\pi w_s^2} \quad \text{Eq. 5}$$

The beam radius can be calculated as a function of distance from the focal position Δz [38]:

$$w_s(z) = \sqrt{w_0^2 + \frac{\Delta z^2 \alpha^2}{4}} \quad \text{Eq. 6}$$

where α is the beam divergence of caustic propagation and can be estimated as d_c/f, where d_c is the collimated beam size and *f* is the focal length of the focusing lens.
Ablation threshold can be a useful indicator for comparing the different interaction conditions between single beam and two-beam interactions. Liu's model describes the diameter of the ablated region as a function of the single pulse energy, with assumptions of a laser beam with a Gaussian distribution, TEM_{00} and a pulse duration shorter than lattice heating time [39]:

$$D^2 = 2w_s^2 \ln\left(\frac{F}{F_{th}}\right) \quad \text{Eq. 7}$$

where F_{th} is the threshold fluence. For ablation with multiple pulses, influence of damage accumulation effect should also be considered. Damage accumulation phenomenon leads to a reduction of threshold fluence, which can be described as [40],[41]:

$$F_{th}(N) = F_{th}(1)N^{S-1} \quad \text{Eq. 8}$$

where N is the number of pulses, $F_{th}(1)$ is the threshold fluence for a single pulse and S is the incubation coefficient related to processed material. Eq.7 can be rewritten to include the damage accumulation as:

$$D^2 = 2w_s^2 \ln\left(\frac{F}{F_{th}(1)N^{S-1}}\right) \quad \text{Eq. 9}$$

Concerning specifically a single Gaussian beam and multiple laser pulses, the Eq.9 can be rewritten with estimated material characteristics as:

$$D^2 = 2w_s^2 \ln\left(\frac{F_m}{\widehat{F_{th,1}}(1)N^{\widehat{S_1}-1}}\right) \quad \text{Eq. 10}$$

where, $\widehat{F_{th,1}}(1)$ and $\hat{S}_1$ are the estimated threshold fluence and the incubation coefficient in case of single Gaussian beam. Considering DLIP process with two beams configuration, the following adaptation of Liu's ablation model is proposed:

$$D_P{}^2 = 2w_s^2 \ln\left(\frac{F_m}{\widehat{F_{th,2}}(1)N^{\widehat{S_2}-1}}\right) \quad \text{Eq. 11}$$

where D_P is the patterned region diameter, and $\widehat{F_{th,2}}(1)$ and $\hat{S}_2$ are respectively the estimated threshold fluence and the incubation coefficient.

3 Materials and Methods

3.1 Materials

AZ31 Mg alloy cold rolled sheets with a thickness of 0.2 mm were used throughout the study. The nominal chemical composition is summarized in Table 1.

3.2 DLIP system

A nanosecond pulsed fiber laser was used throughout the study (YLPG-5, by IPG Photonics, Oxford, MA, USA). Laser source is based on master oscillator power amplifier (MOPA). The laser emits green light at 532 nm, obtained by a conversion from the fundamental wavelength of 1064 nm. The features of the laser source are summarized in Table 2. The laser source produced a ramped emission profile, which was characterized prior to experimentation. The laser source modulation was obtained by means of a function generator (Sony-Tektronix AFG310). The collimated laser beam obtained from the laser source output was split into two beams through a beam splitter. Two folding mirrors allow for the interference between the two beams with a definable angle producing a fringes pattern. Then the two collimated beams were focalized on the sample, using two focal lenses with 100 mm focal length. In order to vary the focal position of laser beams, a micrometric stage in z direction was used with 10 μm resolution. A schematization of the two-beam DLIP setup is reported in Figure 1.

3.3 Experimental procedure

3.3.1 Laser emission profile characterization

As seen in Figure 2, the emission profile of the laser is characterized by an initial ramp, where pulses do not have the same energy content. During this transitory phase, two different regions can be identified. The first region is the delay between the modulation signal and the beginning of the pulses. The second region is characterized by the pulses ramp, with the energy content growing up to a constant value of stability. In the delayed pulses phase, pulses have less than 10% of the average pulse energy in regime. The stable region is assumed to start when ramp profile pulses achieved 90% of regime energy. The laser was driven by means a modulation signal to produce N_{tot} number of pulses, where N_{delay} number of pulses are absent due to the initial delay. Accordingly, the number of pulses within the commanded modulation duration is:

$$N = N_{tot} - N_{delay} \quad \text{Eq. 12}$$

On the other hand, the stable pulse energy E_{st} could be calculated from the average power for the stable regime from the following expression:

$$E_{st} = \frac{P_{avg}}{PRR} \quad \text{Eq. 13}$$

where P_{avg} is the measured average power and PRR is the pulse repetition rate. The energy content of the pulses in the ramped region can be calculated from the acquired oscilloscope traces. Considering the i_{th} pulse, the pulse energy E_i can be expressed as:

$$E_i = E_{st}\frac{A_i}{A_{st}} \quad \text{Eq. 14}$$

where A_i is the discrete integral of the ramped pulse trace and A_{st} the average discrete integral of the stable pulses in regime. For a ramped pulsed train composed of N pulses, the average energy E_m can be expressed as:

$$E_m = \frac{1}{N}\sum_{i=1}^{N} E_i \quad \text{Eq. 15}$$

The ramped pulse train profiles were acquired using an InGasAs fast photodiode (Thorlabs FGA10) and recorded with a digital oscilloscope (Tektronix TDS5034B). The laser source was characterised for different pump current (PI%) and pulse repetition rate (PRR) levels. Five replications were produced for each condition and the number of delayed pulses (N_{delay}) and the number of ramped pulses (N) were measured. Tested experimental conditions are reported in Table 3.

3.3.2 Ablation characteristics with a single Gaussian beam

Ablation characteristics as function of pulse energy (E_m) and number of pulses (N) were studied for both single Gaussian beam and two-beam DLIP configurations. Experimental conditions were reported in Table 4. Three replications were made for each combination. A 3D optical profilometer, based on focus variation microscopy (InfiniteFocus from Alicona Imaging GmbH, Graz, Austria), was used for measuring the ablated diameter. Ablation threshold fluence and incubation coefficient were calculated through non-linear regression fitting.

3.3.3 Two-beam DLIP feasibility window investigation

The low melting point and the use of ns-pulsed laser source generate limited feasibility for effective processing of AZ31 through two-beam DLIP. Accordingly, processing conditions were varied to evaluate the feasibility region in which periodic structures are realized with a high resolution. Laser pulse energy (E_m), number of pulses (N) and focal position (Δz) were varied. The angle between the two laser beams (θ) and the pulse repetition rate were fixed at 37° and 20 kHz respectively. In Table 5 experimental conditions of two-beam DLIP feasibility window investigation are reported. Feasibility process map was determined by a qualitative analysis with SEM technique (EVO-50 from Carl Zeiss, Oberkochen, Germany), in order to classify the different experimental conditions as a function periodic structure presence.

3.3.4 Two-beam DLIP quality characterization

A second experimental campaign was conducted within the determined feasibility window. Energy (E_{st}), number of pulses (N_{tot}) and focal position (Δz) were varied maintaining pulse repletion rate

(PRR) fixed to 20 kHz. In this case, the angle between the two interfering beams (θ) was also varied in order to test its influence on the process and to define limits in working a low melting point material. Ablation threshold and incubation coefficient were estimated through non-linear regression fitting. Pattern period was evaluated on SEM images, measuring the distance among five periodic grooves for all treatments and it was compared to the theoretical value. Ablated region diameter was also measured. Table 6 reports the fixed and variable parameters of this experimental campaign.

4 Results and discussion

4.1 Laser Emission profile characterization

In Figure 3, the characterization of the laser emission profile as a function of laser parameters is reported. Particularly, number of delay pulses and ramp pulses for different machine conditions (PI% and PRR) are considered with the corresponding standard deviation values. It could be deduced that with PRR=20 kHz the laser emission is stabilized with the least number of delayed and ramp pulses. Moreover, the standard deviation of the delayed and ramp pulses for this PRR value was relatively small, pointing at a more stable emission condition overall. Accordingly, the PRR value was fixed at 20 kHz for the rest of the experiments.

4.2 Ablation characteristics of the material with a single Gaussian beam

For single Gaussian beam configuration, the dimple diameter varied between 15 μm and 30 μm, in a range around the theoretical Gaussian beam diameter of 21.7 μm. The increase in dimple diameters as a function of the number of pulses can be attributed to either an increasing pulse energy content and the damage accumulation associated to multiple pulses. A fitting of the experimental data with the Liu's model was performed using the theoretical value of beam waist w_0 equal to 10.9 μm. Within this approximation, the results of the non-linear regression were $\widehat{F_{th,1}}(1) = 0.22 \pm 0.04\ \mathrm{J/cm^2}$ and $\widehat{S_1} = 0.85 \pm 0.06$.

4.3 Two-beam DLIP feasibility window

Experimental conditions were classified in different groups with four identified surface conditions, namely:

- Non treated (NT) surface: conditions below or around the ablation threshold providing no significant changes on the surface;
- Low treated (LT) surface: conditions above ablation threshold generating surface damage without well-defined periodic structures;
- Periodic structures (PS) surface: Surfaces with well-defined periodic structures;
- Melted (M) surface: surfaces with a considerable amount of molten material due to the excessive fluence, which result in the closure of the periodic patterns.

An example for each condition is reported in Figure 4, where feasibility maps are also shown. Feasibility analysis revealed a total absence of interference patterns when lowest pulse energy (9.5

μJ) was used. Where most of the conditions were classified as NT and only for low Δz values, it was possible to observe some treated surfaces but classified as M for the higher fluence. Maintaining constant E_{st}, an increase of Δz is associated to a decrease of fluence, considering that energy value is distributed on a larger spot area. On the other hand, low values of Δz generate a Gaussian distribution with higher fluence with the same energy content (Figure 5-a). With the use of ns laser pulses, molten material can form easily and consequently cover the interference pattern and this is due to the low melting point (905 K) of the magnesium alloy. In a similar fashion, fluence can be reduced by reducing pulse energy with constant Δz (Figure 5-b). As a matter of fact, feasibility window analysis revealed that the PS region was limited and consisted in E_{st}=14.5 - 20 μJ; N_{tot}=16-47, Δz=2.0 - 2.5 mm.

4.4 Ablation characteristics of the material with two-beam DLIP

Figure 6 reports SEM images of the ablated regions as a function of two-beam DLIP parameters. It is possible to assess that all process parameters influenced in different way the measured spot diameter. As a matter of fact, D_p was affected by two-beam set-up configuration; the angle between two beams realize an elliptical shape of spots for axis projection. In particular, an increase in θ resulted in a decrease of D_p; this occurred because the beam spot area grew when θ increased, inducing low fluence values. The same considerations could be done for E_{st}; indeed, since laser energy and fluence are proportional, D_p values increase with E_{st}. Concerning Δz, its rise induced both a growth of beam spot diameter, so of the treated area, and a reduction of process fluence. However, the effect of fluence reduction seems to be stronger in these measurements; for this reason, D_p decreased with an increase of Δz. Moreover, the parameter N_{tot} had an evident effect on D_p, because an increase of N_{tot} means an increase on energy content and so higher D_p values.
Within the feasibility window of the two-beam DLIP process, the ablated region diameter varied between 10 μm and 40 μm. Moreover, the obtained ablated region deviated from a circular shape towards an elliptical one due to inclination angle of the impinging beams. The average diameter of the ellipse was used for the calculation. The estimated threshold fluence were $\widehat{F_{th,2}}(1) = 0.18 \pm 0.03\ \mathrm{J/cm^2}$ and $\widehat{S_2} = 0.99 \pm 0.05$.
In Figure 7, the fluence thresholds and incubation coefficients for the two optical configurations are compared. In terms of the ablation threshold, there is no a statistical difference between two optical configurations. On the other hand, damage incubation is higher in the case of a single Gaussian beam, depicted by the lower coefficient. This statistical results are directly related to the assumptions made in the analysis. In Figure 8, the normalized fluence distribution of single Gaussian beam and the intensity distribution of two-beam DLIP configuration are compared. It is clearly visible that in cases of constructive interference, beams intensity became higher in comparison with intensity of the single beam causing the melting of a large portion of material. This observation is in accordance with models described in paragraph 2.1. Considering an arbitrary value of F_{th} it is possible observed obtained spot size for two-beam DLIP configuration. On the other hand, a comparison with single Gaussian beam configuration revels a lower fluence threshold value in the same condition of spot size. This means an underestimation in $\widehat{F_{th,2}}(1)$ value, which is connected to the assumption of Gaussian profile in fitted Liu's model.

4.5 Effect of process parameters on pattern quality

Periodic structures generated by interference phenomena are affected by laser parameters As a matter of fact, structures quality, in terms of homogeneity distribution and definition, is influenced by process parameters but also by source properties. Spot energy distribution, which is directly connected to beam quality (M^2 factor), determines a non-uniform treatment. In Figure 9, an example of a defect related to laser energy distribution is shown. Periodic structures are clearly visible and well defined on the annulus area. Moving towards the central part of beam spot it is possible to determine a breaking point where features vanish, producing a discontinuous treatment on laser spot. The changed trend in the distribution of the periodic structures is directly related to the quasi-Gaussian energy trend of the laser spot, which causes a higher energy content in the middle part of the spot. In fact, the central part of laser spot showed melting phenomenon and sub-micro features were covered by molten material, in comparison with the annulus which was characterized by a lower energy content. Considering this aspect, in several conditions, when fluence was increased by a change of laser parameters, the central area was characterized by stronger phenomena and, in this case, melting effect was not negligible.

Periodic structures are also affected by laser process parameters. Energy density can be increased varying directly energy level E_{st}, but also changing number of pulses N_{tot} and focal position Δz. Increasing energy content, it was possible to observe a transition from NT to LT conditions and with higher values to PS and M ones. Increasing N_{tot}, energy density increased resulting in larger treated spots and more defined periodic structures. Particularly, Δz strongly affected the process since it is characterized by an inverse proportionality with energy content. An increase of Δz reduced the average fluence and conducted to NT and LT conditions. On the contrary, a decrease of Δz greatly increased the average fluence and conducted to PS and M conditions, as previously described.

Some considerations can be also done about the influence of beams angle on periodic structures quality and its relationship with energy content. In Figure 10, the period of the features is plotted as a function of the average fluence F_m and the angle between the beams. Each group was characterized by a mean value and its relative standard deviation. The plots evidence the effect of fluence factor and consequently of laser parameters on pattern structures. As a matter of fact, the period is determined by Eq. 1 testifying its dependence only by laser wavelength and beams angle. On the other hand, the increase of beams angle corresponds to a reduction in the period pattern dimension and it is associated to a smaller range of fluence F_m values. This affects the feasibility of small period structures. In case of smaller period, the influence of melting phenomena became much more important and it corresponds to a reduction of the feasibility window. Two-beam DLIP fluence range became more limited with decreasing angle. With an increased fluence, the amount of molten phase increases with the number of ns pulses. Moreover, an overall increase of energy density occurs both in regions under constructive and destructive inference. Resultantly, a larger ablated area with absence of interference pattern is generated. Hence, the pattern definition is lost more easily employing high fluence levels with reduced angles.

Pattern periodicity was evaluated through the SEM images. On each SEM image, 5 locations were measured, while the measurement was repeated three times and the average value of them was taken. Figure 11 shows average values and standard deviations for all interference pattern period measurements as function of the angle θ. Average measured values were similar to theoretical ones. Differences are due to both measurement errors and misalignments in the optical setup. However, two-beam DLIP fluence range became more limited with decreasing angle.

5 Discussion

Pattern quality is an important factor regulating the performance of the textured surface in the biomedical application. During a laser surface texturing operation chemical composition, texture shape and texture dimension are altered together. All of these aspects have an impact on the biological performance. Pattern shape has been the mainly investigated aspects, where linear patterns were found to improve endothelial cell adhesion and proliferation [42]-[45]. Cells have also been found to align along the pattern direction, which is further enhanced when sub-micrometric dimensions are achieved on the surface. In particular, different cells prefer differently different pattern size [42]- [45]. Ding et all. investigated line-likes patterns with different period dimensions. In this study, structures with a dimension of 1 μm increased adhesion and proliferation of endothelial cells. Differently, smooth muscle cells were suppressed in spreading and growth [45].
Concerning a biodegradable Mg-alloy, the sub-micrometric surface structure would enhance the biological behaviour of the implant at the initial stages of its use. These linear structures can be exploited to enhance cell adhesion and also alignment especially on cardiovascular stents, where endothelial cells adhesion is required. The small dimensions of the texture should also allow for a reduced damage on the material, not inducing negative effects on the fatigue behaviour. As the biodegradation progresses, the surface texture is expected to be among the first features to disappear. Its influence on the biodegradation behaviour needs further investigations, since degradation behaviour can be modified due to the increased surface area, variations of surface chemistry, and wettability. Texture affects wettability and its scale dimension tunes surface response from hydrophilic behaviour to hydrophobic one. This aspect can be also used in order to promote the adhesion of a protective layer to increase degradation performance of devices.
Considering biomedical fields pattern design is a crucial factor in order to obtain a defined performance. The present work shows the use of linear patterns obtained through a DLIP configuration composed of 2 beams. More complex pattern shapes are achievable through the increase of the number of beams. The use of more complex patterns can be exploited also for parallel manufacturing of micrometric features such as micro dimples, which can favour osseointegration of biodegradable orthopaedic implants.

6 Conclusions

In the present work, a two-beam optical setup was employed in order to obtain a two-beam DLIP process on a difficult to be laser processed AZ31 magnesium alloy. Two-beam DLIP process was realized using an industrial nanosecond fiber laser source with a ramp profile emission. This laser source is characterised by long pulse duration, which are detrimental when materials with low melting temperature are processed. On the other hand, the high pulse energy and frequency guarantee high productivity on large area. Therefore, the role of the threshold fluence and process parameters on the quality of the AZ31 structured surface have to be investigated. Influence of laser parameters in terms of energy, angle between beams, focal position and number of pulses was investigated. A feasibility process window was determined for the material and it appeared to be narrow because of its low melting temperature, constituting low processability. Within the feasibility window, further experimentation was carried out to assess pattern quality and ablation characteristics. The main outcomes are as follows:

- Process feasibility for two-beam DLIP depends highly on the laser diameter. It was found out that defocusing is useful for lowering peak intensity of the interfering beams. In particular, defocusing between 2 to 2.5 mm, sub-micrometric structures could be achieved.
- Ablation behaviour differs between a single Gaussian beam and a two-beam DLIP configuration for AZ31. While the threshold fluence remains statistically unvaried, with a single beam damage incubation was found to be higher.
- Within the feasibility window periodic structures from 1.2 μm down to 600 nm were achieved. While, smaller structures are theoretically possible, period structure definition was reduced with larger angle between the beams due to the inevitable melt generation filling in the generated structures.
- Pattern period depended only on the angle between the beams, while fluence and number of pulses did not induce any significant effect.

The results confirm the effectiveness of the two-beam DLIP method for obtaining micrometric to sub-micrometric surface structures on the low processability AZ31 magnesium alloy. Future attempts will be dedicated to the upscaling of the process for faster and larger area patterning with the described method for industrial manufacturing. In particular, this two-beam DLIP method could be implemented in laser structuring of medical devices in biodegradable magnesium alloy especially stents, but also larger devices such as screws, plates and fasteners, in order to tailor the surface biocompatibility and degradation.

Acknowledgements

The authors would like to acknowledge IPG Photonics Italy for the long-standing collaboration and the laser source loan.

References

[1] F. A. Lasagni, A. F. Lasagni, Fabrication and Characterization in Micro-Nano Range, Springer, New York, 2011.
[2] K. M. T. Ahmmed, C. Grambow, A. Kietzig, Fabrication od Micro/nano Structures on Metals by Femtosecond Laser Micromachining, Micromachines 5 (2014) 1219–1253.
[3] T. Li, M. Paliy, X. Wang, B. Kobe, W. Lau, J. Yang, Facile One-Step Photolithographic Method for Engineering Hierarchically Nano/Microstructured Transparent Superamphiphobic Surfaces, App. Mater. Interfaces 7 (2015) 10988–10992.
[4] N. A. Cinel, S. Cakmakyapan, S. Butun, G. Ertas, E. Ozbay, E-Beam lithography designed substrates for surface enhanced Raman spectroscopy, Photonic Nanostruct. 15 (2015) 109–115.

[5] N. Tanaka, H. Ota, K. Fukumori, J. Miyake, M. Yamato, Micro-patterned cell-sheets fabricated with stamping-force- controlled micro-contact printing, Biomaterials 35(37) (2014) 9802–9810.
[6] Y. Li, H. W. Ng, B. D. Gates, C. Menon, Material versatility using replica molding for large-scale fabrication of high aspect-ratio, high density arrays of nano-pillars, Nanotechnology 25(285303) (2014) 1–10.
[7] Q. Liu, X. Duan, C. Peng, Novel Optical Technologies for Nanofabrication, Springer, New York, 2014.
[8] V. Rui, Laser Surface Modification of Biomaterials Techniques and Applications. Elsevier, 2016.
[9] L. Li, M. Hong, M. Schmidt, M. Zhong, A. Malshe, B. Huis in'tVeld, V. Kovalenko, Laser nano-manufacturing – State of the art and challenges. CIRP Annals - Manufacturing Technology, 60(2), (2011) 735–755.
[10] A. F. Lasagni, D. Yuan, P. Shao, S. Das, Periodic Micropatterning of Polyethylene Glycol Diacrylate Hydrogel by Laser Interference Lithography Using Nano- and Femtosecond Pulsed Lasers, Adv. Eng. Mater. 11(3) (2009) 20–24.
[11] K. M. T. Ahmmed, E. Jee, Y. Ling, P. Servio, A. Kietzig, Introducing a new optimization tool for femtosecond laser-induced surface texturing on titanium, stainless steel, aluminum and copper, Opt. Laser Eng. 66 (2015) 258–268.
[12] B. K. Nayak, M. C. Gupta, Self-organized micro / nano structures in metal surfaces by ultrafast laser irradiation, Opt. Laser Eng. 48(10) (2010) 940–949.
[13] B. M. Duarte, A. Lasagni, R. Giovanelli, J. Narciso, E. Louis, F. Mücklich, Increasing Lubricant Film Lifetime by Grooving Periodical Patterns Using Laser Interference Metallurgy, Adv. Eng. Mater. 10(6) (2008) 554–558.
[14] B. Voisiat, M. Gedvilas, S. Indrišiunas, G. Raciukaitis, Picosecond-Laser 4-Beam-Interference Ablation as a Flexible Tool for Thin Film Microstructuring, Phys. Procedia 12 (2011) 116–124.
[15] X. Li, D. H. Feng, T. Q. Jia, H. Y. He, P. X. Xiong, S. S. Hou, K. Zhou, Z. R. Sun, Z. Xu, Fabrication of a two-dimensional periodic microflower array by three interfered femtosecond laser pulses on Al : ZnO thin films, New. J. Phys. 12 (2010) 1–8.
[16] B. Tan, N. R. Sivakumar, Direct grating writing using femtosecond laser interference fringes formed at the focal point, J. Opt. A-Pure Appl. Op. 7 (2005) 169–174.
[17] J. Huang, S. Beckemper, A. Gillner, K. Wang, Tunable surface texturing by interference, J. Micromech. Microeng. 20 (2010) 1–6.
[18] A. F. Lasagni, D. F. Acevedo, C. A. Barbero, F. Mucklich, Advanced design of conductive polymeric arrays with controlled electrical resistance, Appl. Phys. A Mater. Sci. Process. 91 (2008) 369–373.
[19] F. Lasagni, P. Shao, J. L. Hendricks, C. M. Shaw, D. C. Martin, S. Das, Direct fabrication of periodic patterns with hierarchical sub-wavelength structures on poly (3,4-ethylene dioxythiophene)–poly(styrene sulfonate) thin films using femtosecond laser interference patterning, Appl. Surf. Sci. 256 (2010) 1708–1713.
[20] L. Müller-Meskamp, Y. H. Kim, T. Roch, S. Hofmann, R. Scholz, S. Eckardt, K. Leo, A. F. Lasagni, Efficiency Enhancement of Organic Solar Cells by Fabricating Periodic Surface Textures using Direct Laser Interference Patterning, Adv. Mater. 24 (2012) 906–910.
[21] A. Lasagni, C. Holzapfel, F. Mu, Production of two-dimensional periodical structures by laser interference irradiation on bi-layered metallic thin films, Appl. Surf. Sci. 253 (2006) 1555–1560.
[22] M. D'Alessandria, A. Lasagni, F. Mu, Direct micro-patterning of aluminum substrates via laser interference metallurgy, Appl. Surf. Sci. 255 (2008) 3210–3216.
[23] M. Bieda, C. Schmådicke, T. Roch, A. Lasagni, Ultra-Low Friction on 100Cr6-Steel Surfaces After Direct Laser Interference Patterning, Adv. Eng. Mater. 17 (1) (2015) 102-108.

[24] L. Muller-Meskamp, S. Schubert, T. Roch, S. Eckhardt, K. Leo, A. F. Lasagni, Transparent Conductive Metal Thin-Film Electrodes Structured by Direct Laser Interference Patterning, Adv. Eng. Mater. 17(8) (2015) 1215–1219.
[25] C. Gachot, U. Schmid, F. Mucklich, R. Catrin, A. Lasagni, Comparative study of grain sizes and orientation in microstructured Au, Pt and W thin films designed by laser interference metallurgy, Appl. Surf. Sci. 255 (2009) 5626–5632.
[26] S. Eckhardt, C. Sachse, A. F. Lasagni, Light management in transparent conducting oxides by direct fabrication of periodic surface arrays. Phys. Procedia, 41 (2013) 552–557.
[27] D. Guenther, J. Valle, S. Burgui, C. Gil, C. Solano, A. Toledo-Arana, R. Helbig, C. Warner, I. Lasa, A. F. Lasagni, Direct Laser Interference Patterning for decreased bacterial attachment, Proc. of SPIE 9736 (2016) 1–9.
[28] J. Marczak, J. Kusinski, R. Major, A. Rycyk, A. Sarzynski, M. Strzelec, K. Czyz, Laser interference patterning of diamond-like carbon layers for directed migration and growth of smooth muscle cell depositions, Opt. Appl. XLIV(4) (2014) 575–588.
[29] P. Li, U. Bakowsky, F. Yu, C. Loehbach, F. Muecklich, C.-M. Lehr, Laser Ablation Patterning by Interference Induces Directional Cell Growth, IEEE T. Nanobiosci. 2(3) (2003) 138–145.
[30] E. A. Bremus-koebberling, S. Beckemper, B. Koch, A. Gillner, Nano structures via laser interference patterning for guided cell growth of neuronal cells, J. Laser Appl. 24 (2012) 0420131–0420136.
[31] C. Zwahr, D. Günther, T. Brinkmann, N. Gulow, S. Oswald, G. M. Holthaus, A. F. Lasagni, Laser Surface Pattering of Titanium for Improving the Biological Performance of Dental Implants. Adv. Healthc. Mater. (2017) 1–9.
[32] A. Kurella, N. B. Dahotre, Review paper: Surface Modification for Bioimplants: The Role of Laser Surface, J. Biomater. Appl. 20, (2005) 1–50.
[33] C. Taltavull, B. Torres, a. J. Lopez, P. Rodrigo, E. Otero, A. Atrens, J. Rams, Corrosion behaviour of laser surface melted magnesium alloy AZ91D, Mater. Des. 57 (2014) 40–50.
[34] D. Dube, M. Fiset, A. Couture, I. Nakatsugawa, Characterization and performance of laser melted AZ91D and AM60B, Mat. Sci. Eng. A 299(1-2) (2001) 38–45, 2001.
[35] A. G. Demir, V. Furlan, N. Lecis, B. Previtali, V. Furlan, Laser surface structuring of AZ31 Mg alloy for controlled wettability, Biointerphases 9(2) (2014) 0290091–10.
[36] V. Furlan, A. G. Demir, B. Previtali, Micro and sub-micron surface structuring of AZ31 by laser re-melting and dimpling, Opt. Laser Technol. 75 (2015) 164–172.
[37] E. W. M. Born, Principles of optics electromagnetic theory of propagation, interference and diffraction of light, Cambridge University Press, London, 2005.
[38] H. Huegel, F. Dausinger, Handbook of the Euro-Laser Academy, Volume 2, 1st Edition, 1998.
[39] J. M. Liu, Simple technique for measurements of pulsed Gaussian-beam spot sizes, Opt. Lett. 7(5) (1982) 1980–1982.
[40] Y. Jee, M. F. Becker, R. M. Walser, Laser-induced damage on single-crystal metal surfaces. J. Opt. Soc. Am. B, 5(3) (1988) 648–659.
[41] P. T. Mannion, J. Magee, E. Coyne, G. M. O. Connor, T. J. Glynn, The effect of damage accumulation behaviour on ablation thresholds and damage morphology in ultrafast laser micro-machining of common metals in air, Appl. Surf. Sci. 233 (2004) 275–287.
[42] D. Khang, J. Lu, C. Yao, K. M. Haberstroh, T. J. Webster, The role of nanometer and sub-micron surface features on vascular and bone cell adhesion on titanium. Biomaterials, 29 (2008) 970–983.
[43] P. Vandrangi, S. C. Gott, R. Kozaka, V. G. J. Rodgers, M. P. Rao, Comparative Endothelial Cell Response on Topographically Patterned Titanium and Silicon Substrates with Micrometer to Sub-Micrometer Feature Sizes. Plos One, 9(10) (2014) 1–13.
[44] J. Lu, M. P. Rao, N. C. Macdonald, D. Khang, T. J. Webster, Improved endothelial cell adhesion and proliferation on patterned titanium surfaces with rationally designed , micrometer to nanometer features. Acta Biomater., 4 (2008) 192–201.

[45] Y. Ding, Z. Yang, C. W. C. Bi, M. Yang, S. L. Xu, X. Lu, L. Xiong, N. Huang, P. Huang, Y. Leng, Directing Vascular Cell Selectivity and Hemocompatibility on Patterned Platforms Featuring Variable Topographic Geometry and Size. Appl. Mater. Interfaces, 6 (2014) 12062–12070.

List of tables

Elements	Mg	Al	Mn	Zn	Ca	Si	Cu	Ni	Fe	Others
wt%	bal.	2.5-3.5	0.20	0.6-1.4	0.04	0.10	0.05	0.005	0.005	0.30

Table 1 Chemical composition of employed material

Wavelength	λ	532 nm
Pulse duration	τ	1.2 ns
Pulse repetition rate	PRR	20-300 kHz
Beam quality factor	M_2	1.12
Maximum average power	P_{avg}	6 W
Collimated diameter	d_c	3.492 mm

Table 2 Main characteristics of employed laser source

Fixed parameters		
Modulation time	t_{mod}	3 ms
Varied parameters		
Pump current	PI%	79.3 % - 87.3% - 93.9% - 100%
Pulse Repetition Rate	PRR	20 kHz – 160 kHz – 300 kHz

Table 3 Experimental conditions of laser emission profile characterization

Fixed Parameters		
Pulse Repetition Rate	PRR	20 kHz
Focal Position	Δz	0 mm
Varied parameters		
Energy with single Gaussian beam configuration	$E_{st,1beam}$	5.5 μJ, 11 μJ, 16 μJ, 22 μJ
Energy with two-beam DLIP configuration	$E_{st,2beams}$	4.5 μJ, 9.5 μJ, 14.5 μJ, 20 μJ
Number of pulses	N_{tot}	5, 15, 25, 35, 45

Table 4 Experimental conditions of material ablation characterization

Fixed Parameters		
Pulse repetition rate	PRR	20 kHz
Angle between beams	θ	37°
Varied parameters		
Pulse Energy	E_{st}	3 levels: 9.5 μJ, 14.5 μJ, 20 μJ
Number of pulses	N_{tot}	6 levels: 20, 26, 33, 41, 50, 60
Defocusing	Δz	7 levels: 0.5, 1, 1.5, 2, 2.5, 3, 3.5 mm

Table 5 Experimental conditions of two-beam DLIP feasibility window characterization

Fixed Parameters		
Pulse repetition rate	PRR	20 kHz
Varied parameters		
Pulse Energy	E_{st}	2 levels: 14.5 μJ, 20 μJ
Number of pulses	N_{tot}	6 levels: 33, 41, 50, 60, 70, 80
Defocusing	Δz	3 levels: 2, 2.25, 2.5 mm
Angle between two beams	θ	3 levels: 26°, 37°, 53°

Table 6 Experimental conditions of two-beam DLIP quality characterization

List of figures

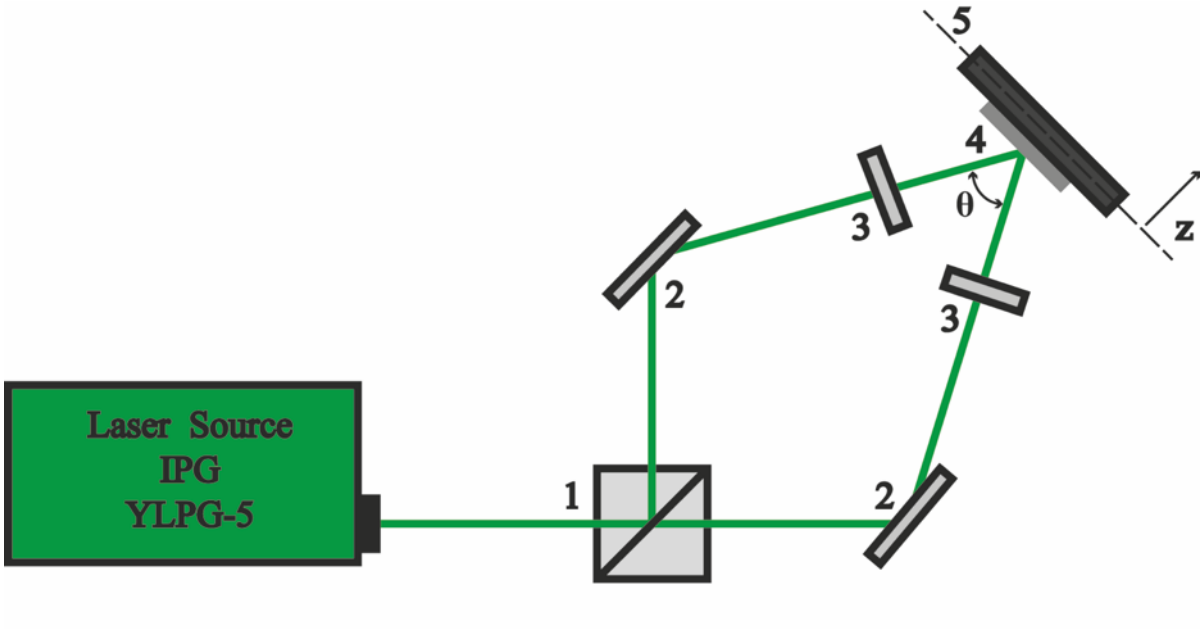

Figure 1 Schematic representation of two-beam DLIP optical setup: 1) beam splitter, 2) mirrors, 3) focal lenses, 4) target plane, 5) z stage

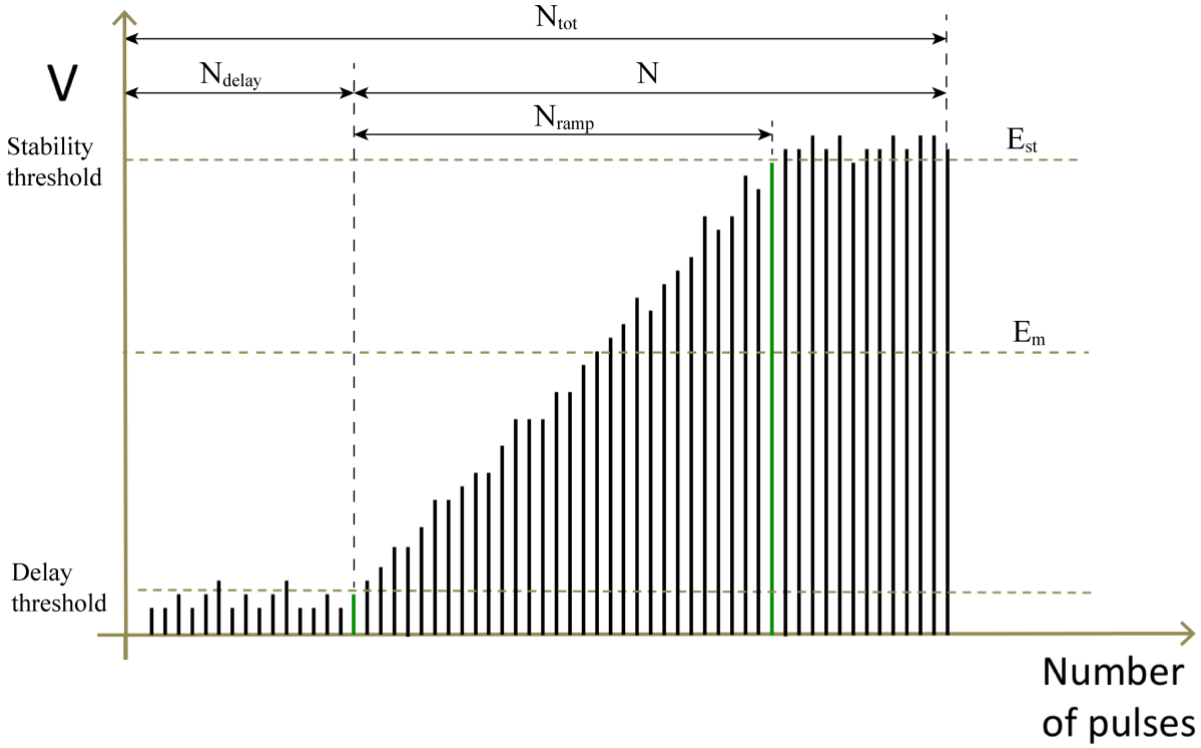

Figure 2 Laser pulsed emission trend for PRR=20 kHz and PI%=100%

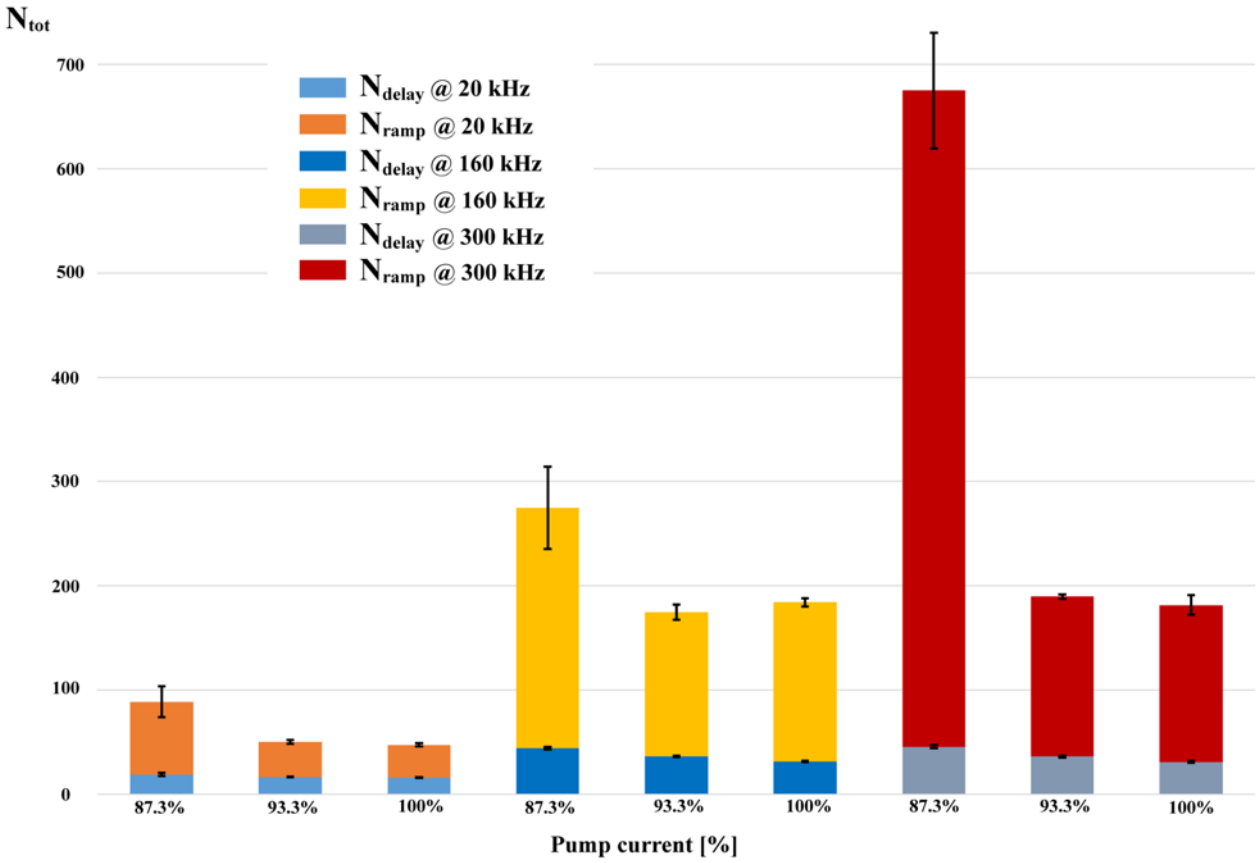

Figure 3 Ramped emission characteristics as function of laser source parameters.

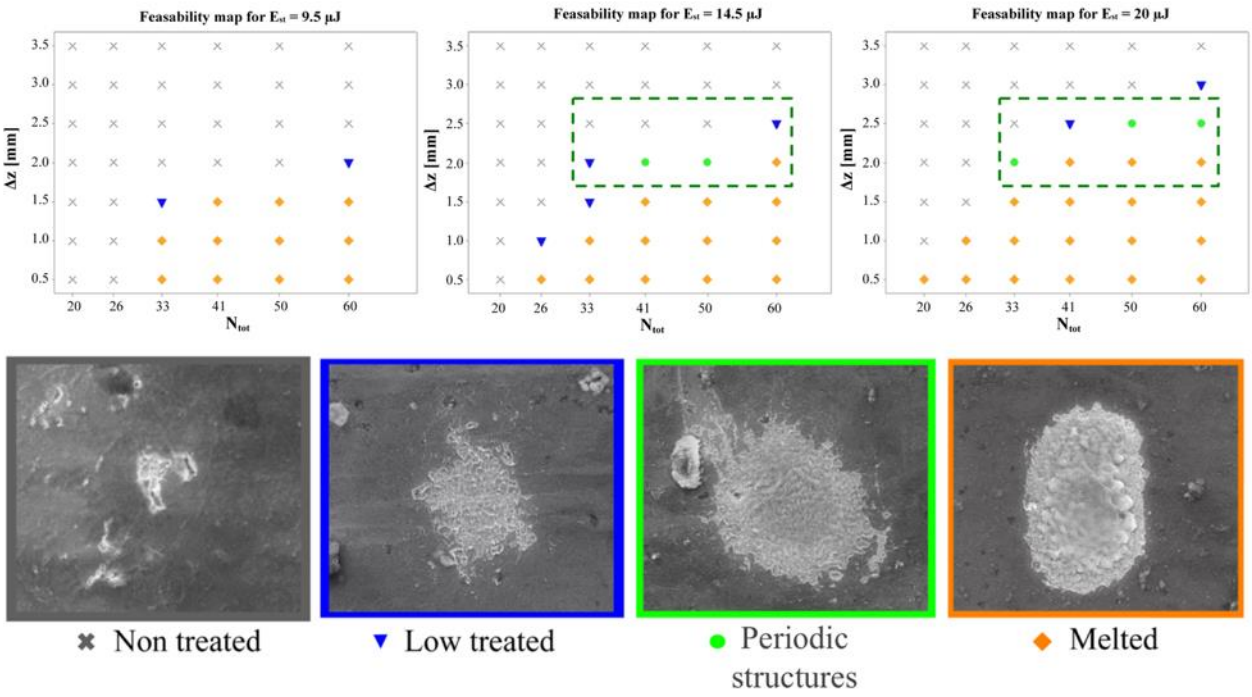

Figure 4 Feasibility map of two-beam DLIP process

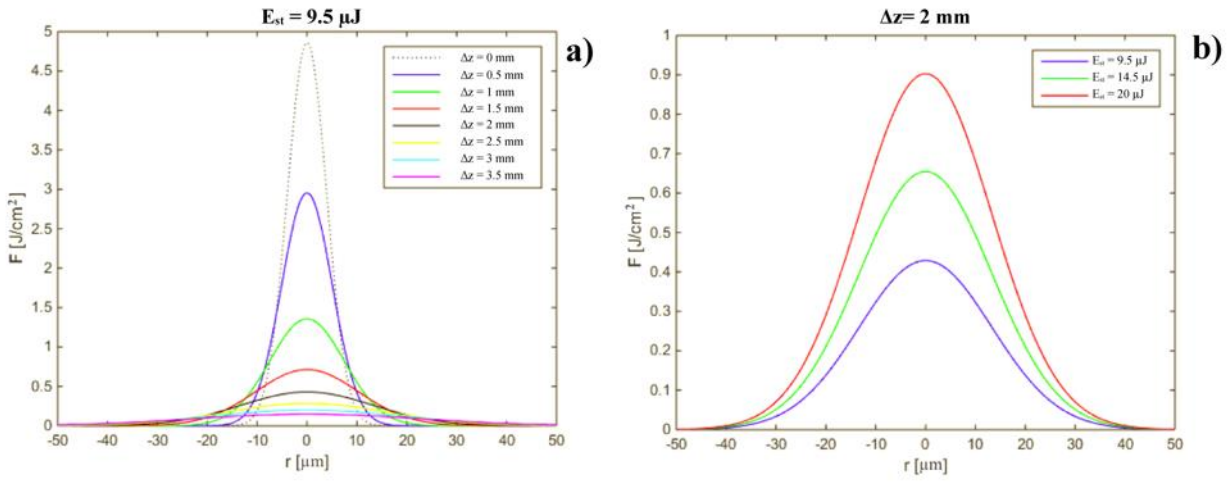

Figure 5 Gaussian profiles: a) constant E_{st} value as a function of different Δz, b) constant Δz value as a function of different E_{st} levels

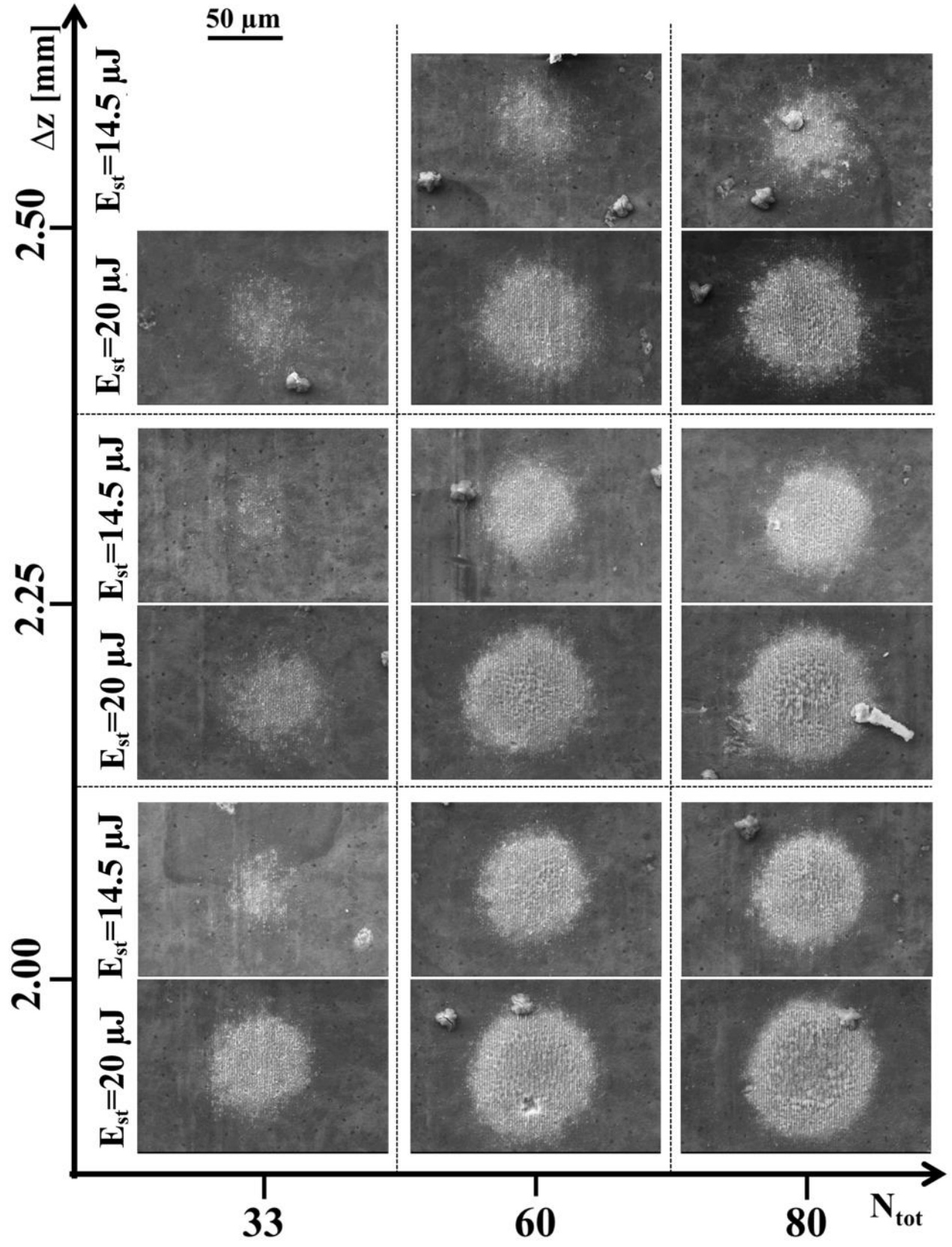

Figure 6 Influence of laser parameters ablated region diameter as function of two-beam DLIP parameters (ϑ=26°).

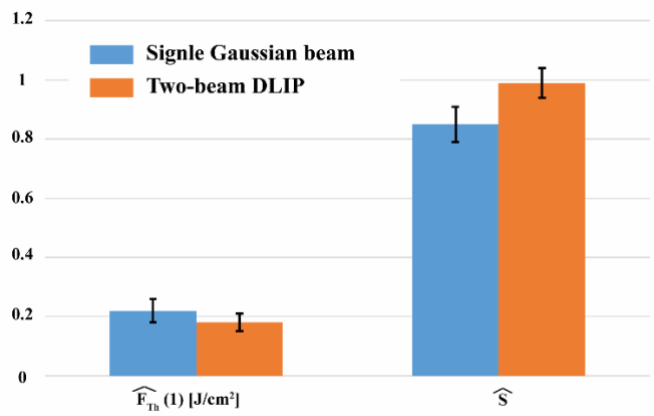

Figure 7. Ablation threshold and incubation coefficient comparison.

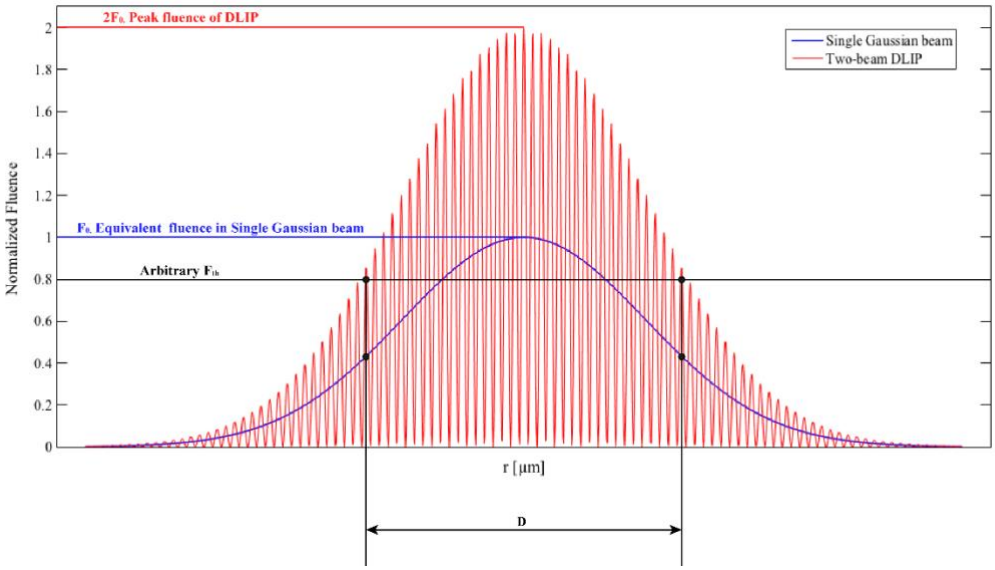

Figure 8 Fluence behaviour considering single Gaussian beam and two-beam DLIP configurations

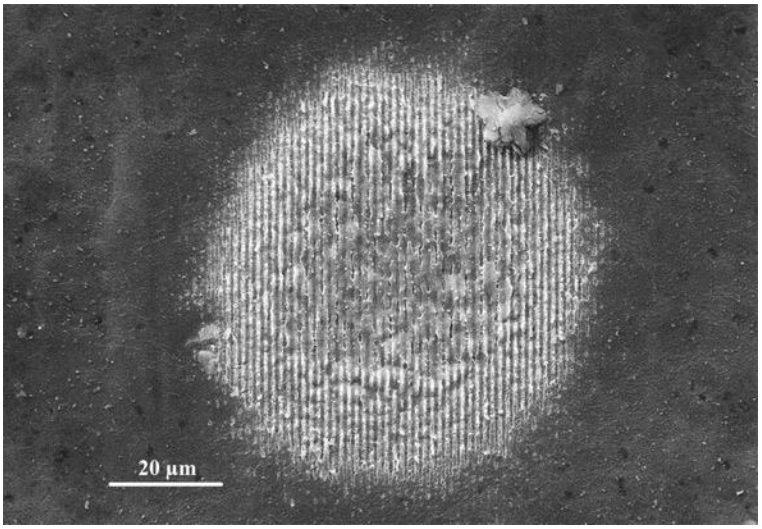

Figure 9 Laser treated spot characterized by E_{st}=20.0 μJ, Δz=2 mm, N_{tot}=80 and θ=26°

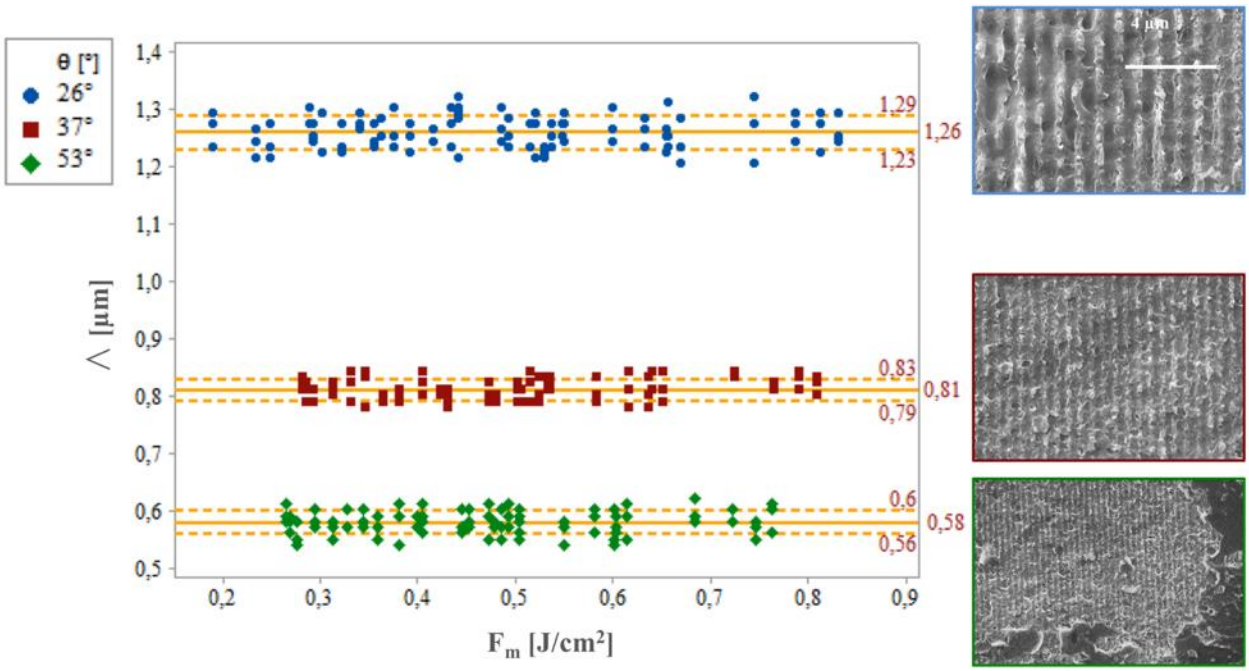

Figure 10 Measured period as a function of average fluence

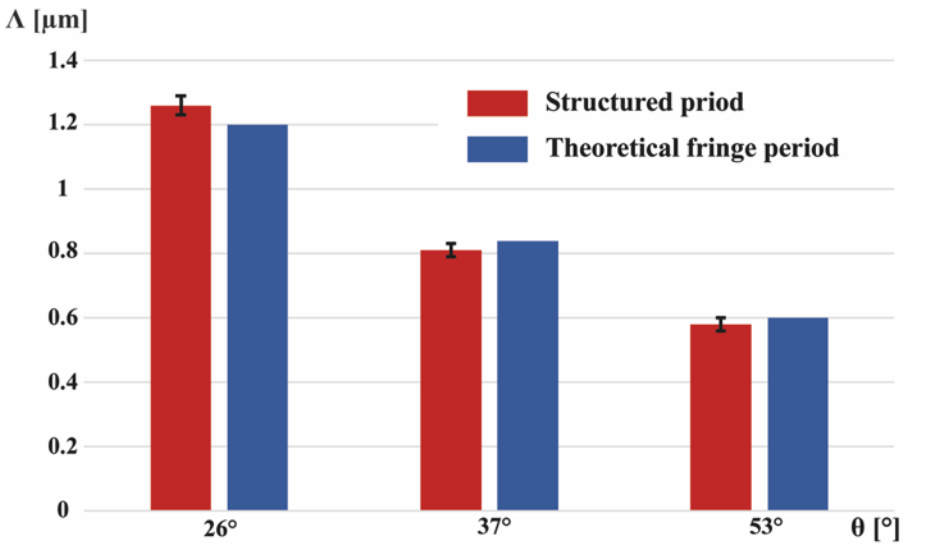

Figure 11 Comparison between measured interference pattern and modelled fringe period